Journal of Hydraulic Research Vol. 00, No. 0 (2003), pp. 1–16

Scour of rock due to the impact of plunging high velocity jets Part II: Experimental results of dynamic pressures at pool bottoms and in one- and two-dimensional closed end rock joints

Affouillement du rocher par impact de jets plongeants à haute vitesse Partie II: Résultats expérimentaux de pressions dynamiques sur le fond de fosses d'affouillement et dans des joints rocheux fermés, uni-et bidimensionnelle

ERIK BOLLAERT, *Senior Research Associate, Laboratory of Hydraulic Constructions, EPFL, CH-1015 Lausanne, Switzerland*
E-mail: erik.bollaert@epfl.ch

ANTON SCHLEISS, *Professor and Director, Laboratory of Hydraulic Constructions, EPFL, CH-1015 Lausanne, Switzerland*
E-mail: anton.schleiss@epfl.ch

ABSTRACT
This paper presents the experimental results of dynamic pressure measurements at simulated plunge pool bottoms and underlying rock joints, due to plunging high velocity jet impact. Emphasis is given on the mean and the fluctuating part of the dynamic pressures, to the extreme pressure values, and to the spectral content of the fluctuations. Particular attention is also paid to the relationship between pool bottom pressures and the pressures they generate inside underlying rock joints. Based on data analysis in one- and two-dimensional rock joints, it was found that high velocity plunging jets are able to generate oscillatory and resonance pressure waves inside the joints. These non-linear transient phenomena propagate at wave celerities that depend on the air content of the air–water mixture inside the joint. This air content is directly related to the plunge pool air content and to instantaneous pressure fluctuations inside the joint. The resulting amplification of pool bottom pressures inside rock joints is believed to be a key for a better assessment of scour formation in rock.

RÉSUMÉ
Le présent article contient les résultats de mesures de pressions dynamiques sur le fond de fosses d'affouillement et à l'intérieur de fissures du rocher artificiellement créées, due à l'impact de jets à haute vitesse. Ceci est fait à l'aide de la moyenne et de l'écart-type des pressions, des valeurs extrêmes et de la fonction de densité énergétique spectrale. Une attention particulière est attribuée à la relation entre les pressions sur le fond de la fosse et les pressions correspondantes à l'intérieur de la fissure. Basé sur l'analyse des mesures dans une fissure unidimensionnelle et une fissure bidimensionnelle, il s'est avéré que des jets à haute vitesse sont capables de générer des conditions de pressions oscillatoires et de résonance à l'intérieur des fissures. Ces phénomènes fortement non-stationnaires et non-linéaires se propagent à des célérités d'onde qui dépendent de la concentration d'air du mélange eau-air dans la fissure. Cette concentration dépend de la quantité d'air dans la fosse même et de la valeur instantanée de la pression dans la fissure. L'amplification des pressions à l'intérieur des fissures constitue un facteur clé pour une meilleure appréhension de la formation de fosses d'affouillement dans des massifs rocheux.

Keywords: Rock scour; high velocity jets; dynamic pressure fluctuations; rock joint pressure amplifications.

1 Introduction

Part I of this paper presents an overview of the state-of-the-art on scour formation in rock, due to the impact of plunging high velocity jets. This state-of-the-art points out the lack of knowledge on the transient and multiphase nature of pressure fluctuations that are responsible for scour formation. Two physical processes are thereby of major importance: (a) hydraulic jacking of the rock mass, causing a progressive break-up of rock joints due to fluctuating pressures, and (b) instantaneous rock block ejection by net pressure differences over and under the blocks.

Integration of these complex processes in a scour evaluation method requires a more detailed knowledge and understanding of transient pressure waves that may possibly occur inside the joints.

A test facility measures fluctuating pressures inside one-dimensional (1D) and two-dimensional (2D) artificially created rock joints, under high velocity jet impact (up to 35 m/s). High data acquisition rates (up to 20 kHz) have been used to identify transient pressure waves. The tested rock joints are closed at their end boundary, focusing on the physical process of hydraulic jacking. Two closed end joint configurations, a 1D form and a 2D

Revision received

form, have been analyzed (Fig. 1). Special attention has been paid to a comparison between pressures at the plunge pool bottom and the resulting pressures inside underlying rock joints. This has been analyzed and discussed in the time, frequency and Strouhal domains.

The pressures measured inside the 1D joint are governed by transient wave phenomena (pressure oscillations, resonance conditions). These phenomena have significant spectral energy at frequencies determined by a joint resonator model with a closed end boundary (fundamental resonance frequency $f_{res} = c/(4 \cdot L_f)$, in which c = celerity and L_f = joint length). This is not surprising given the fact that a high velocity jet impacting a rock joint contains the principal elements of a resonator system: the pressure fluctuations from the jet provide the necessary excitation, while the joint plays the role of resonance volume.

Significant amplification of the spectral energy of the impacting jet occurs inside the joints. This amplification is governed by the transient behavior of the air–water mixture that enters the joint. The air concentration of the mixture and, thus, its compressibility and pressure wave celerity, are directly related to the air concentration in the plunge pool and to the pressure waves traveling through the joint.

2 Experimental facility

2.1 General description

The experimental set-up (Fig. 1) consists of two main parts (Bollaert and Schleiss, 2001a; Bollaert, 2002): (a) a 3 m diameter cylindrical basin in steel reinforced plastic, simulating the plunge pool, and (b) a 1 mm thin steel sheeting, modeling the rock joint. This steel sheeting is pre-stressed between two 100 mm thick steel plates with a weight of 1 ton each. The jet outlet has a cylindrical or convergent shape, for a nozzle diameter of 0.057 or 0.072 m. The installation produces mean jet velocities of maximum 35 m/s. A series of maximum 8 flush-mounted micro pressure sensors (pressure range 0–17 bar, 3 mm diameter diaphragm) simultaneously record dynamic pressure fluctuations at the plunge pool bottom and inside the rock joint, for data acquisition rates of 1–20 kHz. The water depth in the plunge pool can be varied from 0 to 0.9 m. This is sufficient to create a high-velocity diffusing turbulent shear layer that impacts the underlying rock joint.

2.2 Jet characteristics

Jet characteristics for cylindrical nozzles are summarized at Table 1. The tests conducted with convergent nozzles procured similar results and are not presented herein. They can be found in Bollaert (2002). The turbulence intensities at the jet outlet have been measured between 3 and 6%. The observed jets are compact because of their small fall heights (max. 0.50 m) and a small degree of break-up (max. 0.35). However, since secondary flow currents in the supply conduit could not be completely avoided, the jets show some low frequency (<1 Hz) instabilities at jet velocities below 15–20 m/s. These instabilities are particularly visible at small pool depths (<0.50 m). For similar velocity and pool depth conditions, two different forms of jet can be observed: a compact form (FORM A), which occurs most of the time, and an unstable form (FORM B), happening occasionally (Fig. 2).

2.3 Artificially created rock joints

The rock joints are formed by cutting a piece out of a thin steel sheeting. This allows generating joints with any possible geometry, but for a constant thickness. In this paper, the results of a 1D joint (0.80 m long, 0.01 m wide and 0.001 m thick) and a 2D joint (0.80 m long, 0.60 m wide and 0.001 m thick), as illustrated in Fig. 3, are presented and compared. For simplicity, only the steel structure and the position of the impacting jet are shown. The location of the pressure sensor at the pool bottom surface, directly under the jet's centerline, is indicated with "a", the other pool bottom sensors with "a^{ii}" and "a^{iv}". Sensors "b", "c" and "d" are located at the entrance, the middle and the bottom of the joint.

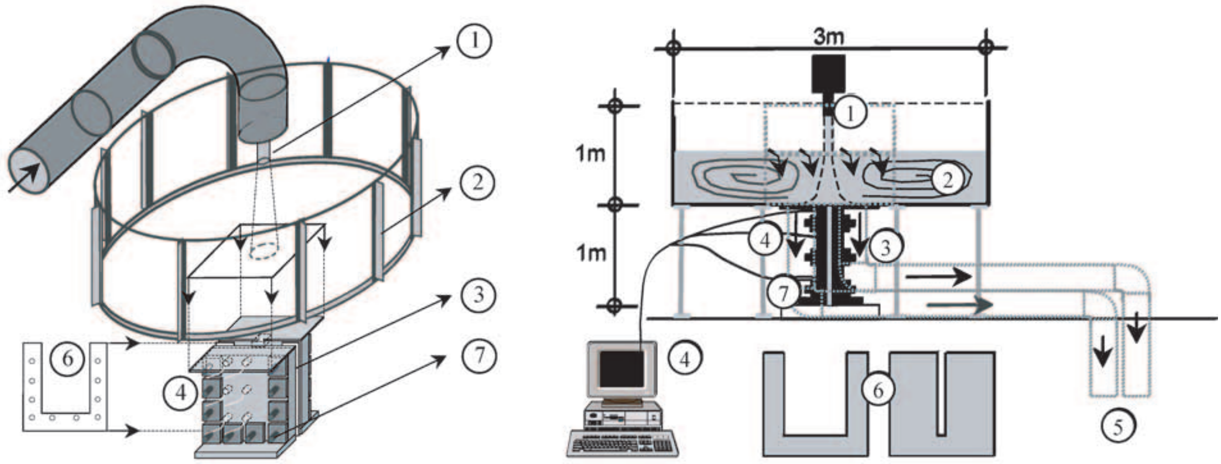

Figure 1 Perspective view and side view of the experimental facility: (1) cylindrical jet outlet, (2) reinforced plastic cylindrical basin, (3) pre-stressed two-plate steel structure, (4) pressure sensors, (5) restitution system, (6) thin steel sheeting pre-stressed between steel structure (defining the form of artificial 1D–2D joints), (7) pre-stressed steel bars.

Table 1 Main characteristics of vertical plunging circular jets.

Jet diam. D_j m	Jet disch. Q l/s	Jet veloc. V_j m/s	Froude number F_j -	Reynolds number Re_j -	Weber number We_j -	Fall height L m	L/D_j -	Pool depth Y m	Y/D_j -	Jet turb. int. Tu %	Breakup length L_b m	Degree of spread $L/L_{b\,max}$ -
0.072	30	7.4	8.8	4.E + 05	232	0.03–0.5	0.4-6.9	0.2–0.7	2.1–9.7	6.3	1.43	0.35
	40	9.8	11.7	5.E + 05	308	0.03–0.5	0.4–6.9	0.2–0.7	2.1–9.7	5.7	1.72	0.29
	50	12.3	14.6	7.E + 05	386	0.03–0.5	0.4–6.9	0.2–0.7	2.1–9.7	5.3	1.98	0.25
	60	14.7	17.5	8.E + 05	462	0.03–0.5	0.4–6.9	0.2–0.7	2.1–9.7	4.6	2.38	0.21
	70	17.2	20.5	1.E + 06	540	0.03–0.5	0.4–6.9	0.2–0.7	2.1-9.7	4.5	2.56	0.20
	80	19.7	23.4	1.E + 06	619	0.03–0.5	0.4–6.9	0.2–0.7	2.1–9.7	4.2	2.86	0.17
	90	22.1	26.3	1.E + 06	694	0.03–0.5	0.4–6.9	0.2–0.7	2.1–9.7	3.8	3.22	0.16
	100	24.6	29.3	1.E + 06	773	0.03–0.5	0.4–6.9	0.2–0.7	2.1–9.7	3.6	3.53	0.14
	110	27	32.1	1.E + 06	848	0.03–0.5	0.4–6.9	0.2–0.7	2.1–9.7	3.7	3.57	0.14
	120	29.5	35.1	2.E + 06	926	0.03–0.5	0.4–6.9	0.2–0.7	2.1–9.7	3.4	3.92	0.13
0.057	20	7.9	9.4	4.E + 05	248	0.03–0.5	0.5–8.8	0.2–0.7	2.5-12.3	–	–	–
	30	11.8	14.0	7.E + 05	371	0.03–0.5	0.5–8.8	0.2–0.7	2.5–12.3	–	–	–
	40	15.7	18.7	9.E + 05	493	0.03–0.5	0.5–8.8	0.2–0.7	2.5–12.3	–	–	–
	50	19.6	23.3	1.E + 06	616	0.03–0.5	0.5–8.8	0.2–0.7	2.5–12.3	–	–	–
	60	23.5	28.0	1.E + 06	738	0.03–0.5	0.5–8.8	0.2–0.7	2.5–12.3	–	–	–
	70	27.4	32.6	2.E + 06	861	0.03–0.5	0.5–8.8	0.2–0.7	2.5–12.3	–	–	–
	80	31.3	37.2	2.E + 06	983	0.03–0.5	0.5–8.8	0.2–0.7	2.5–12.3	–	–	–

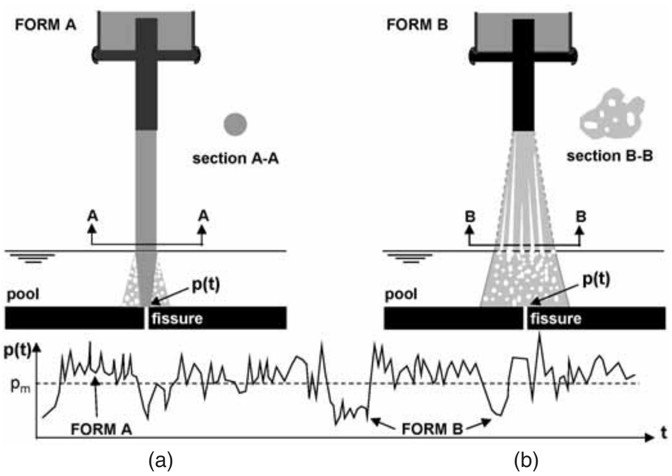

Figure 2 Two types of jet profile are observed at jet velocities <15–20 m/s: (a) compact jet; (b) unstable jet.

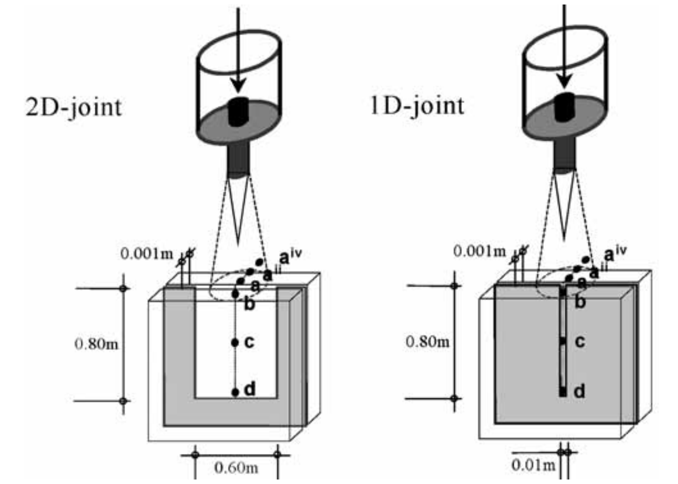

Figure 3 Artificially created closed-end rock joints with location of pressure sensors at the pool bottom (a, a^{ii} and a^{iv}), and inside the rock joint (b, c, d).

3 Flow and pressure conditions

3.1 Diffusive shear layer in plunge pool

The impact of a jet into a pool is governed by jet diffusion through a medium at rest. Momentum exchange with the pool creates a progressively growing shear layer, characterized by an increase of the jet's total cross section and a convergence of the core of the jet (Fig. 4). Dynamic pressures acting at the water–rock interface can be generated by core jet impact, occurring for small plunge pool depths, or by impact of a fully developed macroturbulent shear layer, occurring for ratios of pool depth to jet thickness Y/D_j higher than 4 to 6. The exact Y/D_j ratio dividing these two regimes depends on jet outlet conditions and low-frequency jet stability. For the present study, a value of Y/D_j between 5 and 6 has been deduced from the tests.

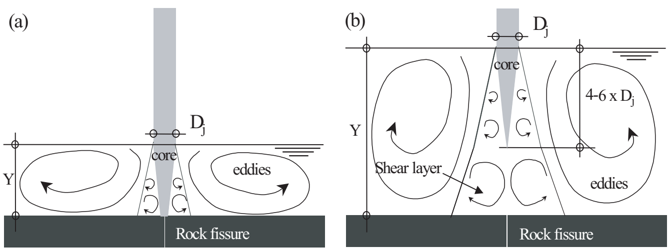

Figure 4 Plunging jets: (a) jet core impact (for Y/D_j < 4–6); (b) developed jet impact (for Y/D_j > 4-6).

Terminology used in this paper distinguishes between core jet impact (Fig. 4a) and developed jet impact (Fig. 4b) (see also Part I of the paper).

3.2 Pressure wave propagation in rock joints

The transfer of pressures from the plunge pool bottom into a rock joint is characterized by a change from macroturbulent flow conditions to pressurized flow through a bounded medium. In the joint, an important transformation of velocity into pressure, i.e. a water hammer phenomenon, occurs.

The impact of a jet onto a rock joint has all the elements necessary to create a resonator system. These resonance capabilities depend on the spectral excitation of the jet. For example, in the case of a pressure wave celerity of $c = 1400$ m/s, jet excitation onto a joint of (maximum) 10 m long can create resonance pressure conditions inside the joint for a frequency range beyond 35–70 Hz, based on the fundamental resonance mode $f_{res} = c/(4 \cdot L_f)$, for a closed end boundary, or $f_{res} = c/(2 \cdot L_f)$, for open end boundaries. This frequency range seems hardly possible to attain in case of macroturbulent flow, which is considered to be governed by large eddies and to possess spectral energy mainly at low frequencies (<20–25 Hz, Toso and Bowers, 1988).

The present tests and previous investigations (Bearman, 1972; Ballio *et al.*, 1992) indicate, however, that high velocity jets have sufficient energy beyond this frequency range to stimulate rock joints to resonance (Part I of this paper).

For pressure wave propagation of the highly compressible air–water mixture inside the rock joints, the steel structure may be considered as very rigid, with a modulus of elasticity of the prestressed steel bars of $E_{st} = 2 \cdot 10^{11}$ GPa.

4 Aeration conditions

4.1 Plunge pool air entrainment

The air concentration at the point of impact of the jet in the plunge pool (α_j) depends on the initial jet turbulence intensity (Tu), the jet velocity (V_j), and the ratio of fall depth to jet diameter (L/D_j). Most of the existing evaluation methods estimate α_j at low jet velocities only (<10–15 m/s). Based on a comparison of air concentrations available in literature, for circular plunging jet impact and for a relatively vast range of jet velocities (Van de Sande and Smith, 1973; Bin, 1984; Ervine *et al.*, 1997; Ervine, 1998), a reasonable extension towards prototype jet velocities has been established. This results in an air concentration α_i that increases almost linearly with jet velocity V_j. Depending on the ratio of jet fall height to jet diameter L/D_j, values for α_j of 25–40% at $V_j = 10$ m/s, and 40–65% at $V_j = 35$ m/s, are theoretically deduced (Fig. 5a).

The highest values correspond to a volumetric air-to-water ratio of $\beta = 1.5$–2, which is very close to the physically plausible maximum value of 2 to 3 (Mason, 1989). Therefore, for the present test facility, a prototype aeration rate is assumed at the point of jet impact in the plunge pool, and no major aeration scale effects are believed to exist.

4.2 Air entrainment in rock joints

A high amount of air is present in the diffusing shear layer of the plunge pool. At the interface with the rock, pressurized flow containing free air, as well as air in solution, penetrates the rock joints. For such a mixture, the change with pressure of the volume α that is occupied by a certain quantity (or mass) of air can be expressed by the equation of state for gases under isothermal conditions as $\alpha \cdot p = \alpha_i \cdot p_i$ (i = initial conditions). In other words, a pressure increase generates a decrease in air volume, provided that the quantity of air remains constant.

Furthermore, during pressure oscillations, the quantity of air may change due to air release or air resolution. If the pressure of a liquid with air in solution suddenly decreases, supersaturation and air release may occur. The opposite effect occurs if the pressure increases. The released amount of air depends on the agitation of the liquid, the presence of nuclei, the amplitude and duration of the pressure drop below the prevailing saturation pressure and the geometry of the joint. The difference with the ideal gas law is that not only the volume but also the quantity (mass) of free air changes as a function of pressure.

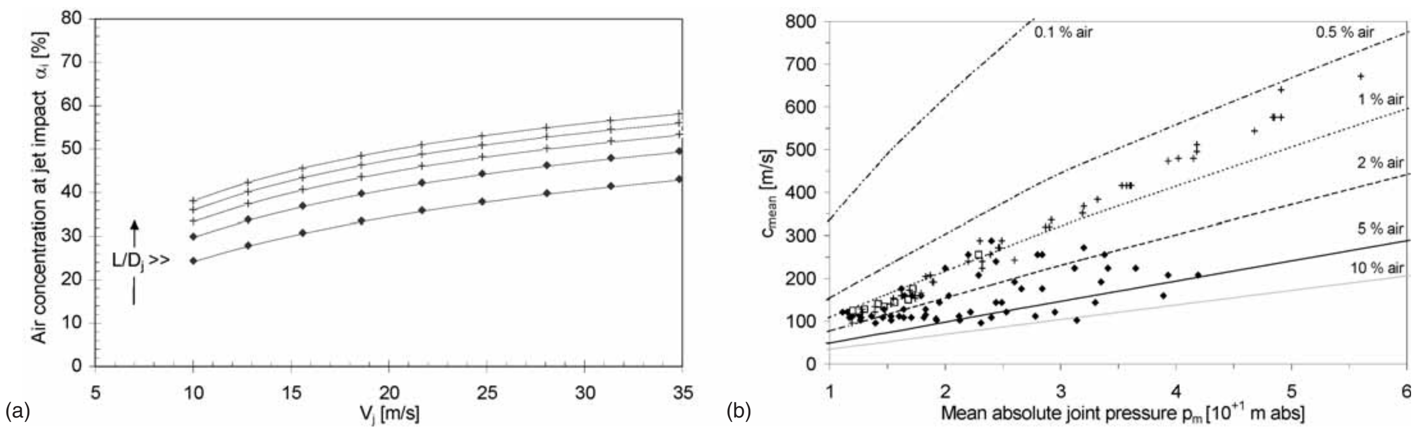

Figure 5 Aeration conditions for submerged (□), core (+) and developed (♦) jet impact conditions: (a) mean plunge pool air concentration α_j at point of jet impact, according to existing theoretical expressions for circular impinging jets; (b) computed mean wave celerity c_{mean} inside one- and two-dimensional rock joints as a function of the mean absolute joint pressure p_m (based on measured fundamental resonance frequency f_{res} in the spectral domain and by assuming $c_{mean} = 4Lf_{res}$).

Therefore, it may be stated that the air concentration inside a rock joint is governed by the air that is available in the plunge pool and by pressure oscillations in the joint. The latter change both the volume and the quantity of free air. While the mass density of an air–water mixture is hardly modified by pressure changes, a slight change in free air content, following a pressure change, drastically modifies the mixture's compressibility and pressure wave celerity.

Figure 5b presents the theoretical relationship between pressure wave celerity c (in [m/s]) and absolute pressure p_{abs} (in [m]) of an air–water mixture, for different air contents (Wylie and Streeter, 1978). The volume of air as indicated on the curves is valid at standard atmospheric pressure conditions only and decreases with increasing pressure. The wall boundaries of the rock joint are considered infinitely rigid.

Figure 5b also presents the relationship between the mean celerity c_{mean} and the mean absolute pressure p_m in the joint, as experimentally derived by pressure measurements (for core and developed jets). The celerities have been derived from the fundamental resonance frequency of the joints. This frequency is defined by the power spectral density of the measured pressures, and by assuming a theoretical fundamental resonance frequency of $f_{res} = c_{mean}/(4 \cdot L_f)$.

Such an approach only procures the average air concentration in the joints and does not allow defining a local and instantaneous celerity-pressure relationship. Due to a continuously changing air content in the joint, the instantaneous resonance frequencies are spread over a wide range of possible frequencies. Therefore, an instantaneous celerity-pressure relationship can only be defined based on space-time correlations taken at high acquisition rates (10 to 20 kHz) and for very short time intervals (typically one pulse). Such correlations are not discussed in the present paper but can be found in Bollaert (2002).

The time-averaged celerity-pressure relationships presented in Fig. 5b are obtained from the tested one- and two-dimensional rock joints and make a clear distinction between submerged, core and developed jet impact conditions.

For submerged and core jet impact, the mean celerity rapidly increases with the mean pressure inside the joint. A comparison with the theoretical curves shows that the mean volume of free air is situated between 0.5 and 1%. Theoretically, no free air should exist within the core of the jet at impact. Also, for tests with a submerged jet, for which no air at all is observed in the plunge pool or the jet, the same statement can be made. This indicates that the free air available inside the joint might be generated by air release during pressure drops, or that the free air was already present inside the joint before jet impact.

On the other hand, developed jet impact produces a mean amount of air in the joint that is significantly higher than for core jets. This results in very low pressure wave celerities. The mean air content increases with the mean pressure in the joint, and values up to 10–20% are observed. This is due to the high air content in the plunge pool and to significant pressure fluctuations inside the joint. Both effects largely increase with increasing jet velocity and mean pressure. Celerities less than 100 m/s have so been deduced from the experiments (Bollaert and Schleiss, 2001a).

5 Spectral analysis of dynamic pressures

5.1 Dynamic pressures at plunge pool bottom

Three pressure sensors ((a), (a^{ii}) and (a^{iv}), see Fig. 3) have been used to measure the turbulent pressure field at the plunge pool bottom. The presented results only apply to the pressure sensor that is located directly under the jet's centerline (sensor (a)). The other two sensors, located radially outwards from the jet's centerline, have pressure characteristics that are qualitatively similar (Bollaert, 2002).

The excitation capacity of a plunging jet can be characterized by its power spectral density S_{xx}. The power spectral density S_{xx} is expressed as a function of frequency f, or as a function of a plunge pool Strouhal number $S_{h,p}$ $(= f \cdot Y/V_j)$. $S_{xx}(f)$ represents a decomposition with frequency of the variance σ^2 of the pressure fluctuations. It can be made dimensionless by dividing it by this variance. This allows visualizing the relative importance of each frequency compared to the total spectral content and has been done in Fig. 6 for core and developed jets.

For core jets, the spectral content is characterized by a linear slope decay of -1, even at high frequencies (beyond 100 Hz) (Fig. 6a). Moreover, it can be seen in Figs. 6a and c that core jet impact cannot be represented in a dimensionless domain. The spectral density curves for different jet velocities only overlap in the dimensional frequency domain. This is because the core of the jet is not affected by the surrounding turbulent shear layer and its related eddy sizes ($\sim$Y) and velocities ($\sim V_j$). Thus, the plunge pool Strouhal number $S_{h,p}$ is of no direct influence on the spectral density of the jet core.

Developed jets produce more spectral energy at low (<20 Hz) and intermediate (20–100 Hz) frequencies. The spectral density suddenly decays at a linear $-7/3$ slope, corresponding to values available in literature (Bearman, 1972; Huot *et al.*, 1986). The inertial subrange of the spectrum decays faster towards the viscous dissipation range than the Von Karman form ($-5/3$ slope, Hinze, 1959) and starts at a frequency that clearly depends on the flow conditions (Fig. 6b). According to the findings of Ballio *et al.* (1994), the $-7/3$ slope of the inertial subrange was found independent of Y/D_j. In the Strouhal domain, the separation point between the two regions of constant spectral decay (slopes of -1 and $-7/3$) corresponds more or less to a Strouhal number $S_{h,p}$ of 1 (Fig. 6d). Developed jet impact is governed by a turbulent shear layer and depends on turbulent eddy sizes, which are defined by the jet velocity V_j and the pool depth Y. Thus, the spectral density for developed jets is correctly presented in a dimensionless domain.

In conclusion, the impact of a high velocity jet may generate significant spectral energy at frequencies that are higher than those typically attributed to macroturbulent flow conditions (0–25 Hz, Toso and Bowers, 1988; see Part I of the paper). This is valid for both core and developed jet impact conditions.

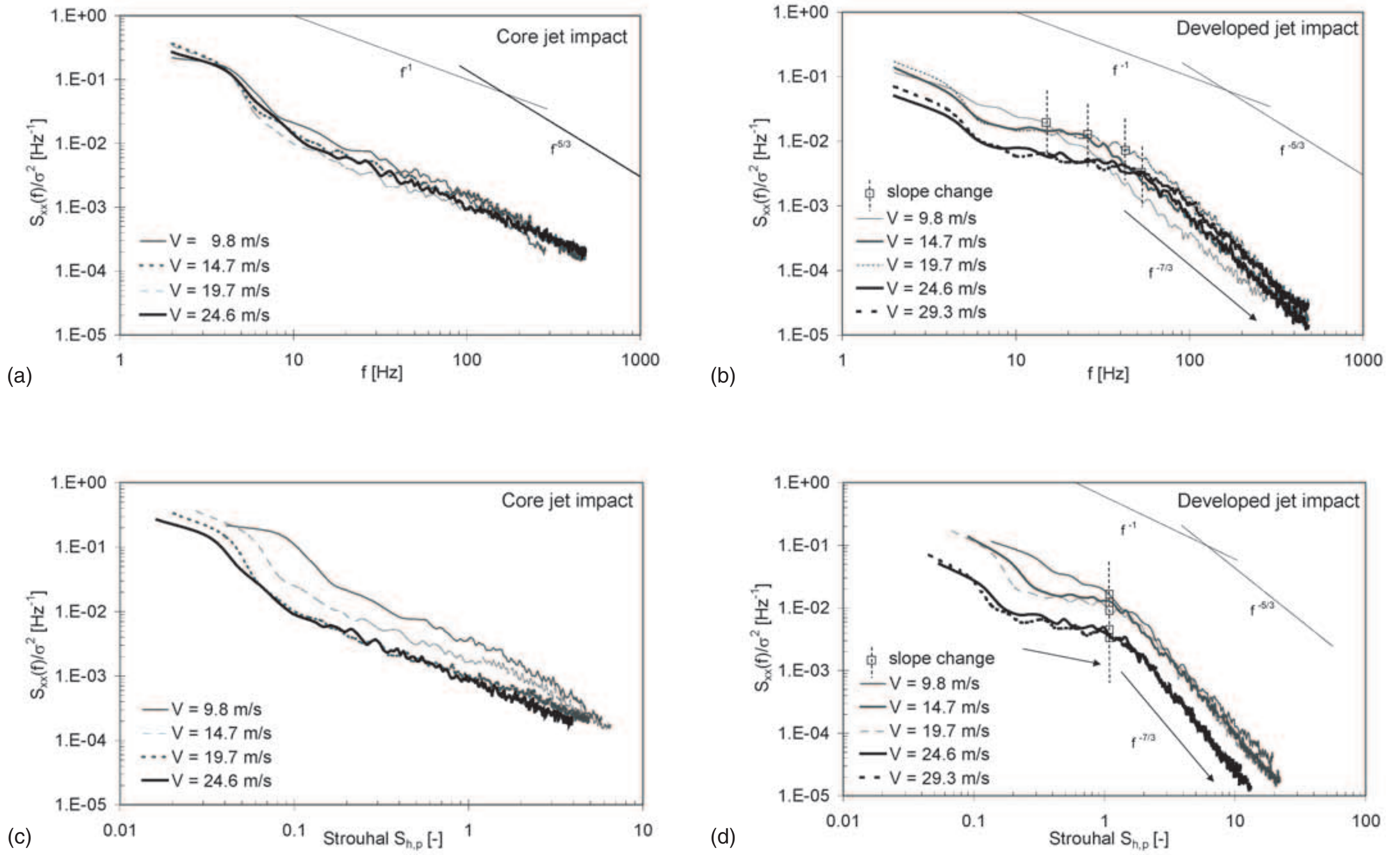

Figure 6 Comparison of dimensionless spectral densities of plunge pool bottom pressures, due to core jet impact (+) or developed jet impact (♦), at sensor (a): (a) core jet impact in frequency domain, (b) developed jet impact in frequency domain, (c) core jet impact in Strouhal domain, (d) developed jet impact in Strouhal domain.

5.2 Dynamic pressures in rock joints

The spectral energy of high velocity jets, presented in §5.1, extends beyond the macroturbulent frequency range and might be able to create oscillatory and resonance pressure conditions inside rock joints. The formation of standing waves and/or resonance conditions may so lead to significant pressure amplifications, resulting in an amplitude and frequency modulation of the spectral density of the incoming pressure fluctuations (Bollaert, 2001). This spectral modulation can be quantified by the amplitude gain of the transfer function between the pressures inside the joint and those at the plunge pool bottom. The amplitude gain expresses the amplitude ratio of the response signal (= rock joint pressure) to the input signal (= plunge pool pressure), for the spectral range of interest. The function defines to which extend, and for which frequencies, pool bottom pressure fluctuations are able to enter and excite the underlying joint.

For the 1D joint, distinction is made between core jet impact and developed jet impact. The left-hand side of Fig. 7 summarizes pressure measurements for a plunge pool depth Y of 0.20 m, corresponding to core jet impact. Figure 7a presents a time-domain comparison between the pool bottom pressures (sensor position (a)) and the pressures measured at the closed end inside the rock joint (sensor position (d)). The signals are recorded for a mean jet velocity of 24.6 m/s. The core of the jet generates a quite constant pressure signal at the entrance of the rock joint. Pressure fluctuations are rare and rather insignificant. For such ideal core jet impact, no air is transferred from the plunge pool into the joint. As a result, the corresponding pressure waves inside the joint propagate at high wave celerities, and the fundamental resonance frequency of the joint is very high. The impacting jet has most of its spectral energy at lower frequencies and, therefore, the response pressure signal inside the joint is weak.

However, the core of the jet occasionally exhibits an instantaneous instability, characterized by a sudden pressure drop at the joint entrance. During this phenomenon, which is generated by low-frequency jet turbulence and jet instability, free air is available in the water that enters the joint. This significantly lowers the pressure wave celerity and corresponding fundamental resonance frequency of the joint. For joint resonance frequencies that lie within the range of spectral excitation of the impacting jet, the pressure response of the joint is violent and generates a quasi-instantaneous peak. The occurrence of peak pressures during core jet impact depends on the number of sudden and short-lived instabilities of the core of the jet. It is believed that real core jets exhibit this phenomenon on a regular basis.

A dimensionless but similar reasoning for core jets is illustrated in Figs. 7c and e, representing respectively the dimensionless spectral density $S_{xx}(f)/\sigma^2$ and the amplitude gain of the transfer function, both expressed as a function of a dimensionless frequency f/f_{res}. The fundamental resonance frequency f_{res} has thereby been determined, based on the amplitude gain and on the first phase shift of the transfer function, as follows.

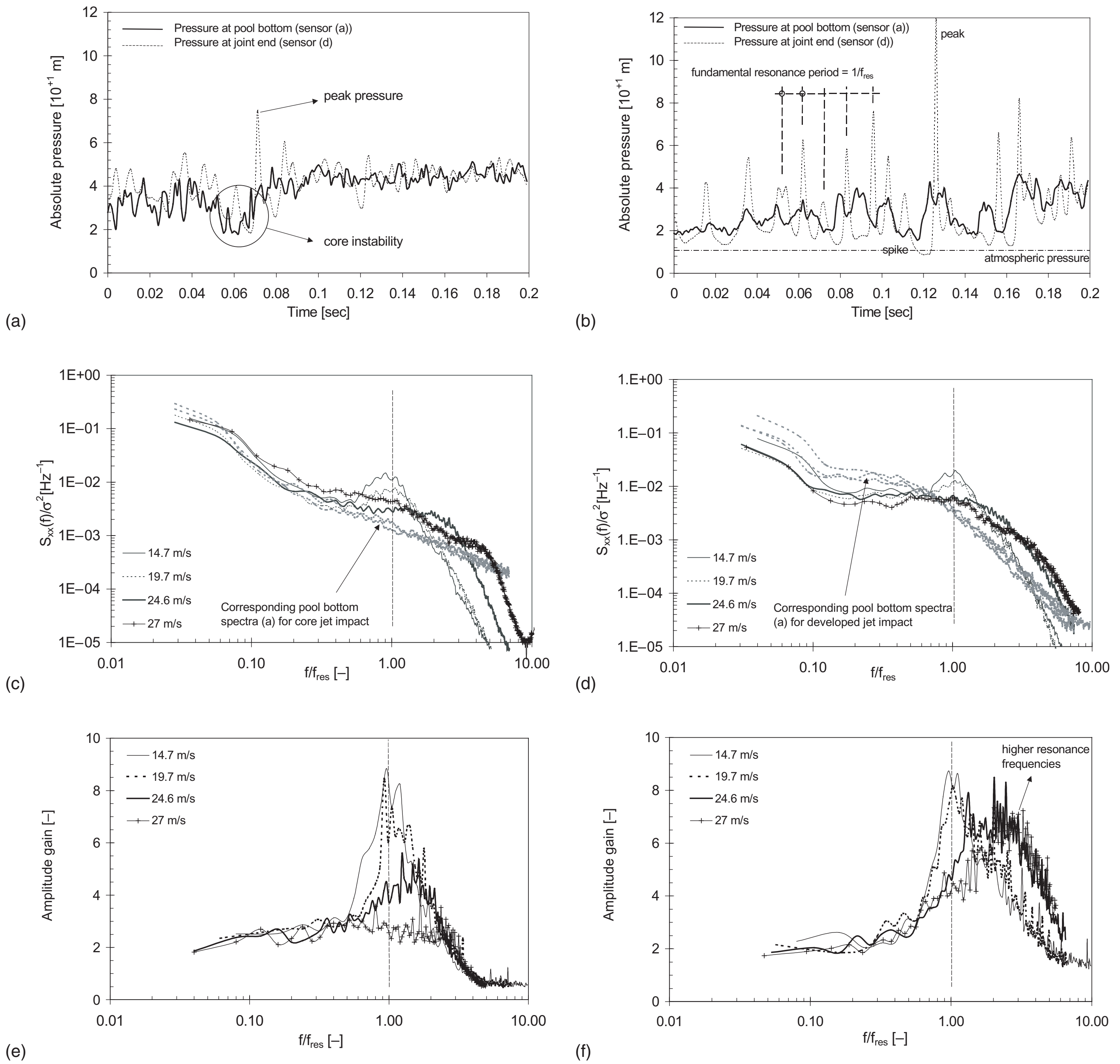

Figure 7 Comparison of dynamic pressure measurements at the plunge pool bottom (near the joint entry) and inside an underlying 1D rock joint (form of the 1D joint is presented in Fig. 3): (a) core jet: time-domain signal for a jet velocity of 24.6 m/s; (b) developed jet: time-domain signal for a jet velocity of 24.6 m/s; (c) core jet: spectral density $S_{xx}(f)/\sigma^2$ as a function of f/f_{res}; (d) developed jet: spectral density $S_{xx}(f)/\sigma^2$ as a function of f/f_{res}; (e) core jet: amplitude gain of the transfer function; (f) developed jet: amplitude gain of the transfer function.

At low jet velocities (<20 m/s), the fundamental resonance frequency of the joint is defined as the frequency at which the amplitude gain of the transfer function becomes maximum. Figure 7e shows that the amplitude gain exhibits a sharp peak around a well-defined frequency for the two lowest jet velocities presented, i.e. 14.7 and 19.7 m/s. Also, the fundamental resonance frequency systematically occurs at the frequency of the first phase shift of the transfer function. This has not been presented herein but can be found in Bollaert (2002). Figure 7e shows that the amplitude gain exhibits a sharp peak around a well-defined frequency for the two lowest jet velocities presented, i.e. 14.7 m/s and 19.7 m/s. This is because the core of the jet exhibits short-lived instabilities (FORM B of Fig. 3) and related pressure drops. Therefore, a certain amount of air is temporarily available in the joint. The pressure changes are rather small and do not significantly change the volume of air in the joint. Also, the wave celerity in the joint is quite low because of the low mean pressure. As a result, the amplitude gain of the transfer function is sharply peaked around a well-expressed mean fundamental resonance frequency.

At higher jet velocities (>20 m/s), sudden pressure changes in the core of the jet can be significant but are rare. Most of the time, an almost constant pressure occurs. Also, only the air present inside the core of the jet is theoretically able to enter the joint. This results in high wave celerities and high resonance frequencies. Although core jets contain some spectral energy at relatively high frequencies (§5.1), the amplitude gain at these frequencies is not significant because the fundamental resonance frequency of the joint is simply too high to be excited by the jet. This results in low amplitude gains of the transfer function.

The right-hand side of Fig. 7 summarizes pressure measurements for developed jet impact (plunge pool depth of 0.67 m). The pressure signals shown in Fig. 7b compare the pool bottom pressures with the pressure response measured at the closed end inside the joint, for a mean jet velocity of 24.6 m/s. The plunge pool bottom pressures are characterized by significant and frequent pressure changes. The pressure at the closed end inside the joint is characterized by an alternation of peak pressures and periods of very low pressures, down to the atmospheric pressure.

The corresponding spectral content (Fig. 7d) looks quite similar to the one measured for core jet impact. However, the transfer function (Fig. 7f) shows that this similarity only holds for low jet velocities (<15–20 m/s). For higher jet velocities, major differences are observed. For such velocities, developed jets generate significant turbulent pressure fluctuations at the entry of the joint. The resulting high air content inside the joint keeps the wave celerities low. This results in fundamental resonance frequencies of the joint system that correspond to frequencies that are easily generated by the impacting jet. Hence, the pressures inside the joint are excited and stimulated to resonance by the pressure fluctuations at their entry.

Also, it may be observed that the fundamental resonance frequency is not well-determined anymore based on the amplitude gain of the transfer function (Fig. 7e). This is due to the continuously changing air content in the joint during pressure fluctuations. A change in air content thereby generates a change in pressure wave celerity and a corresponding change in the fundamental resonance frequency. This non-linear behaviour is the reason why the amplitude gain of the transfer function is not sharply peaked anymore around a well-defined frequency, but spread over a range of possible resonance frequencies. Which frequency is representative for the joint system is hard to define. Therefore, by similarity with low jet velocities, the time-averaged fundamental resonance frequency has been defined at the frequency of the first phase shift of the transfer function. The so defined resonance frequencies were found in good agreement with the typical time period of a complete pressure cycle as defined by a consecution of one peak and one spike.

The appearance of short-lived peak pressures (Fig. 7b) is reflected in the amplitude gain of the transfer function (Fig. 7f): the peaks generate significant amplitude gains at frequencies that are much higher than the time-averaged fundamental resonance frequency f_{res}. Comparison of Fig. 7f (for developed jets) with Fig. 7e (for core jets) shows that, in the latter case, the amplitude gains at high jet velocities are much lower.

As a conclusion, for 1D joints, the amplitude gain of the transfer function is more pronounced for developed jets than for core jets. This difference increases with jet velocity, since, at high jet velocities, only developed jets are able to maintain a high air content inside the joint. This decreases the pressure wave celerity and the corresponding resonance frequency of the joint. For a spectral jet excitation close to the resonance frequency of the joint, significant pressure amplifications occur. The high and constant pressures of core jet impact, on the other hand, prevent the occurrence of a sufficient air content and, therefore, pressure amplifications inside the joint are rare. However, due to instantaneous instabilities of the core of the jet, some air may be entrained into the joint from time to time. When this happens, developed jet impact conditions prevail rather than core jet impact conditions, and some amplification of the input pressure signal may occur.

A similar analysis has been made for a 2D joint. A 2D joint is defined as a joint with a width that is a multiple of the jet diameter at impact D_j. The left- and right-hand sides of Fig. 8 correspond to pressure measurements for core and developed jet impact conditions. All tests, independent of the jet velocity, produce significant air inside the joint. Even in the case of stable core jet impact, the shear layer that surrounds the core is able to continuously transport a significant air content into the 2D joint. As a result, the fundamental resonance frequency of the joint is more or less independent of the jet velocity and of the pressure inside the joint. The corresponding wave celerities have been estimated on the order of 100 m/s. Due to 2D diffusive effects, no significant pressure amplification occurs inside the joint. However, as shown in Fig. 8b for developed jets, the pressure inside the joint can still become higher than the one at the surface. Higher harmonics of the resonance frequency are more visible than for the 1D joint. The reason for this is not clear.

6 Time domain analysis of dynamic pressures

6.1 Dynamic pressures at plunge pool bottom

The dimensionless *mean dynamic pressure* coefficient C_{pa}, measured directly under the jet's centerline (sensor (a)), is defined as a function of the mean dynamic pressure head H_m (= mean pressure minus pool depth Y):

$$C_{pa} = \frac{H_m}{\varphi \cdot V_j^2/2g} \tag{1}$$

The parameter φ accounts for the shape of the velocity profile at the jet outlet. Experimental evaluation of pressure fluctuations at jet issuance revealed values of φ between 1.0 and 1.1.

C_{pa} has been analyzed as a function of the Y/D_j ratio. Figure 9a compares C_{pa} with the best-fit curves of experiments made by Ervine *et al.* (1997) and by Franzetti and Tanda (1987). For core jet impact ($Y/D_j \leq 6$), the measured C_{pa} values are lower than the best-fit curves. This is probably due to the high air entrainment on the present test facility. This air entrainment is estimated at prototype values, due to the applied near-prototype jet velocities (§4.1, Fig. 5a). Also, occasional jet instabilities at low velocities (<15 m/s), caused by the supply conduit, decrease the mean dynamic pressure. It is believed that both aforementioned effects, which are basically scaling and laboratory modeling effects, are

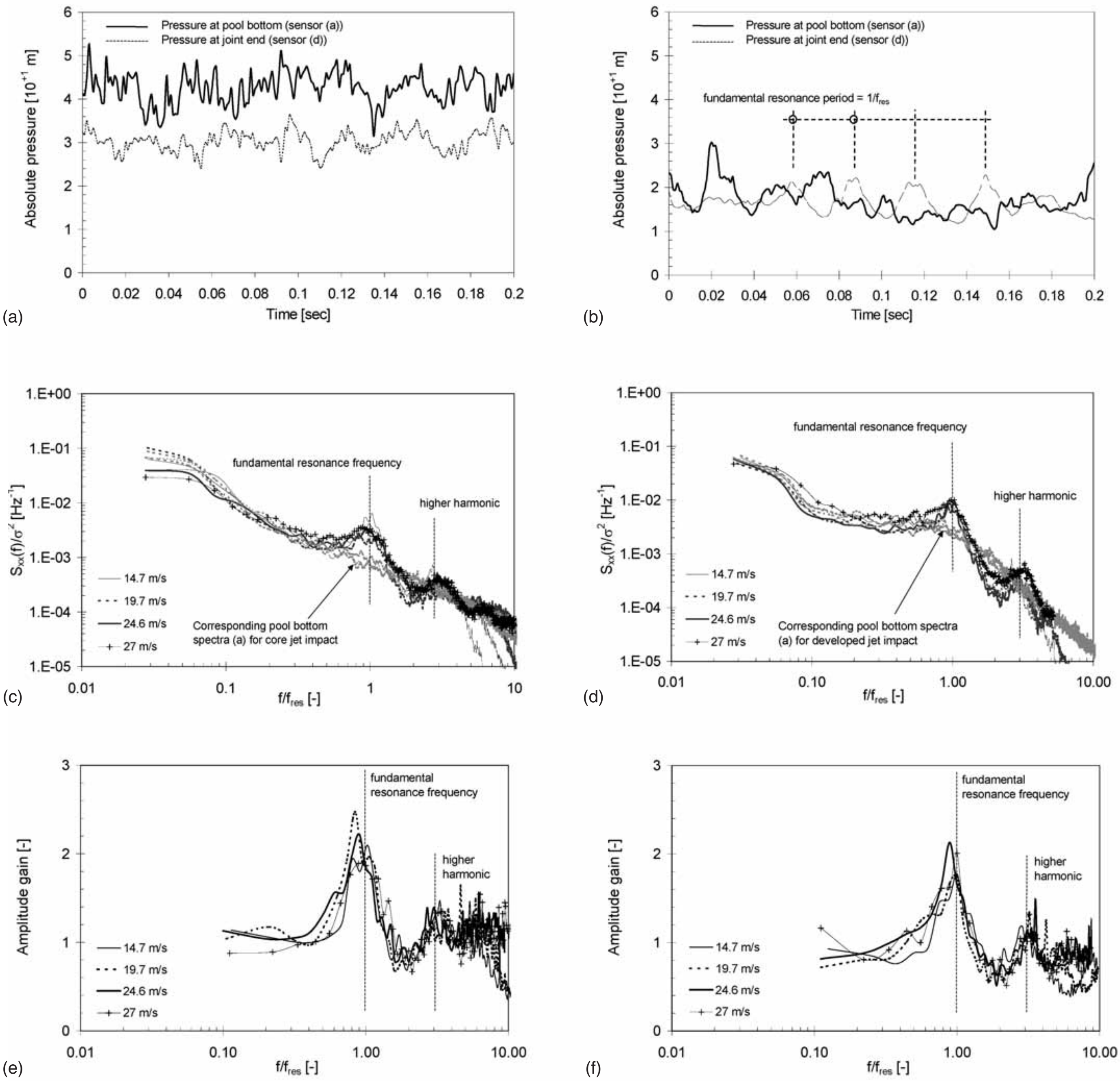

Figure 8 Comparison of dynamic pressure measurements at the plunge pool bottom (near the joint entry) and inside an underlying 2D rock joint (form of the 2D joint is presented in Fig. 3): (a) core jet: time-domain signal for a jet velocity of 24.6 m/s; (b) developed jet: time-domain signal for a jet velocity of 24.6 m/s; (c) core jet: spectral density $S_{xx}(f)/\sigma^2$ as a function of f/f_{res}; (d) developed jet: spectral density $S_{xx}(f)/\sigma^2$ as a function of f/f_{res}; (e) core jet: amplitude gain of the transfer function; (f) developed jet: amplitude gain of the transfer function.

representative for prototype jets. Their influence merits further research.

Figure 10b represents the Y/D_j ratio for a jet diameter of 0.072 m, as a function of the jet velocity V_j. The plunge pool depths Y have been prefixed on the installation between 0.20 and 0.67 m, by means of overflow weirs. The exact water depth observed during the experiments is nevertheless affected by occasional appearance of a surface dimple, due to vortex formation in the cylindrical basin. This decreases the water depth as fixed by the overflow weirs. On the other hand, jet impact diameters D_j were difficult to determine based on visual observations during the experiments. They have been computed based on the jet fall length L and on the jet angle of outer spread δ_{out}. The latter increases with jet velocity. Pool depths of 0.20–0.40 m correspond to $Y/D_j < 6$, for which core jet impact forms. Pool depths of 0.60–0.67 m generate a $Y/D_j > 6$ and correspond to developed jet impact. For a pool depth of 0.50 m, developed jet impact only occurs for jet velocities below 15–20 m/s. For higher velocities, core jet impact was observed, due to the mentioned vortex formation and progressive increase of D_j with increasing jet velocity.

As a conclusion, real-life plunge pool water depths and jet impact diameters may be affected by occasional turbulent vortex formation and/or jet instabilities upon impact. Hence, when using

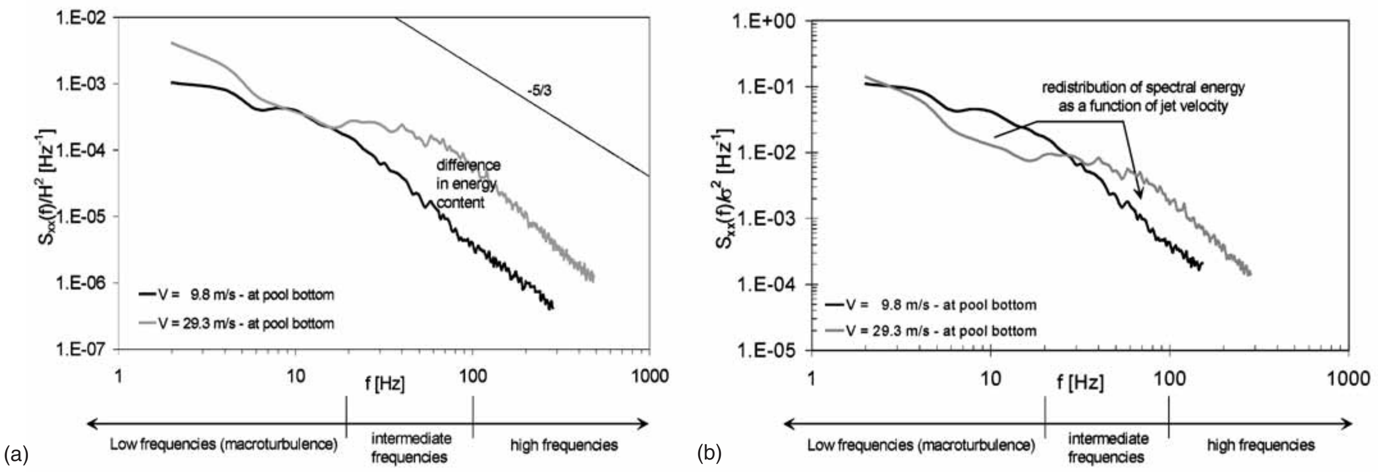

Figure 9 Comparison of spectral content for low and high velocity jets: (a) $S_{xx}(f)$ divided by H^2; (b) $S_{xx}(f)$ divided by σ^2.

the Y/D_j ratio to define the degree of development of the jet and its related pressure fluctuations at the plunge pool bottom, care has to be taken and engineering judgment is necessary.

The importance of *pressure fluctuations around the mean value* is analyzed by means of the root-mean-square (RMS) coefficient C'_{pa}. This coefficient expresses the RMS value of the dynamic pressure fluctuations, H' (in [m]), as a function of the incoming kinetic energy of the jet:

$$C'_{pa} = \frac{H'}{\varphi \cdot V_j^2/2g} \tag{2}$$

These pressure fluctuations have been compared with available literature data (Ervine *et al.*, 1997; Franzetti and Tanda, 1987). Figure 10c shows that C'_{pa} increases for Y/D_j ratios up to 6–7, followed by a continuous decrease, as a result of increasing jet diffusion. In general, the measured C'_{pa} values are higher than predicted by literature data. Comparison with the band width of data given by Ervine *et al.* (1997) shows that the data of the present study are shifted towards higher values. RMS values are defined as the summation (integral) over frequency of the spectral energy content of the flow. Hence, small-scale models have low velocities and cannot correctly simulate the spectral energy of the jet in the intermediate and upper parts of the frequencies. This conducts to RMS values that are too low compared to prototype situations. Due to the near-prototype velocities used in the present study, the intermediate and high frequency parts of the spectrum are believed to be representative for real-life spectra. Therefore, the corresponding RMS values are significantly higher than the ones obtained on scaled model data.

A qualitative and quantitative confirmation of the above statement is presented in Figs. 9a, b and 10d. Figure 10d presents C'_{pa} as a function of jet velocity V_j. At jet velocities less than 20 m/s, the C'_{pa} values generally decrease with decreasing jet velocity. This is particularly visible for developed jet impact conditions. For core jet impact conditions, some RMS values increase with decreasing jet velocity. This is due to the increasing turbulence intensity Tu of the jet with decreasing jet velocity, which is an artifact of the experimental installation. The Tu increase from 3 to 6% is generated by low-frequency jet instabilities, which are predominant at low jet velocities and low water depths (corresponding to core jet impact). These instabilities are generated due to flow conditions in the supply conduit of the experimental facility and their relevance for practice depends on low-frequency jet stability. Jet stability is a topic that has, to the authors' knowledge, never been studied in detail on high-velocity plunging jets and that merits attention in future research. Despite this phenomenon, it is obvious that, for similar geometrical conditions, low jet velocities generate RMS values that are significantly lower than the ones for high jet velocities. Hence, Fig. 10d quantitatively illustrates the spectral difference between a scaled jet model and a prototype jet model.

A qualitative explanation is provided based on Fig. 9, which compares the power spectral content $S_{xx}(f)$ of developed jets as a function of frequency, for jet velocities of 9.8 and 29.3 m/s. Figure 9a presents the ratio of the power spectral content S_{xx} to the square of the incoming energy head of the jet $(\varphi \cdot V^2/2g)^2 = H^2$, in which H stands for the pressure head of the jet at impact (in [m]). This dimensionless power spectral content allows correct comparison of the surfaces under the spectral curves. The surface located in between both curves expresses the difference in dimensionless energy content and confirms the statement that high velocity jets generate more spectral energy than low velocity jets (higher RMS values). Also, the figure illustrates which range of frequencies are directly responsible for this higher energy content. Most frequencies contribute, but the intermediate (20–100 Hz) and high (>100 Hz) frequency ranges are clearly of more significance than the low macroturbulent (<20 Hz) frequency range. This confirms that scaled models with low jet velocities do not correctly simulate intermediate and high frequencies.

Figure 9b presents the same information, but for a ratio of power spectral content S_{xx} to variance of the pressure fluctuations σ^2. As such, eventual differences in RMS (σ^2) values between low and high jet velocities are discarded from the analysis and only qualitative frequency influences are accounted for. Low jet velocities concentrate turbulent energy towards lower frequencies, because they are not able to generate intermediate and high frequencies. High jet velocities redistribute the turbulent energy from lower to higher frequencies. This is summarized at Table 2,

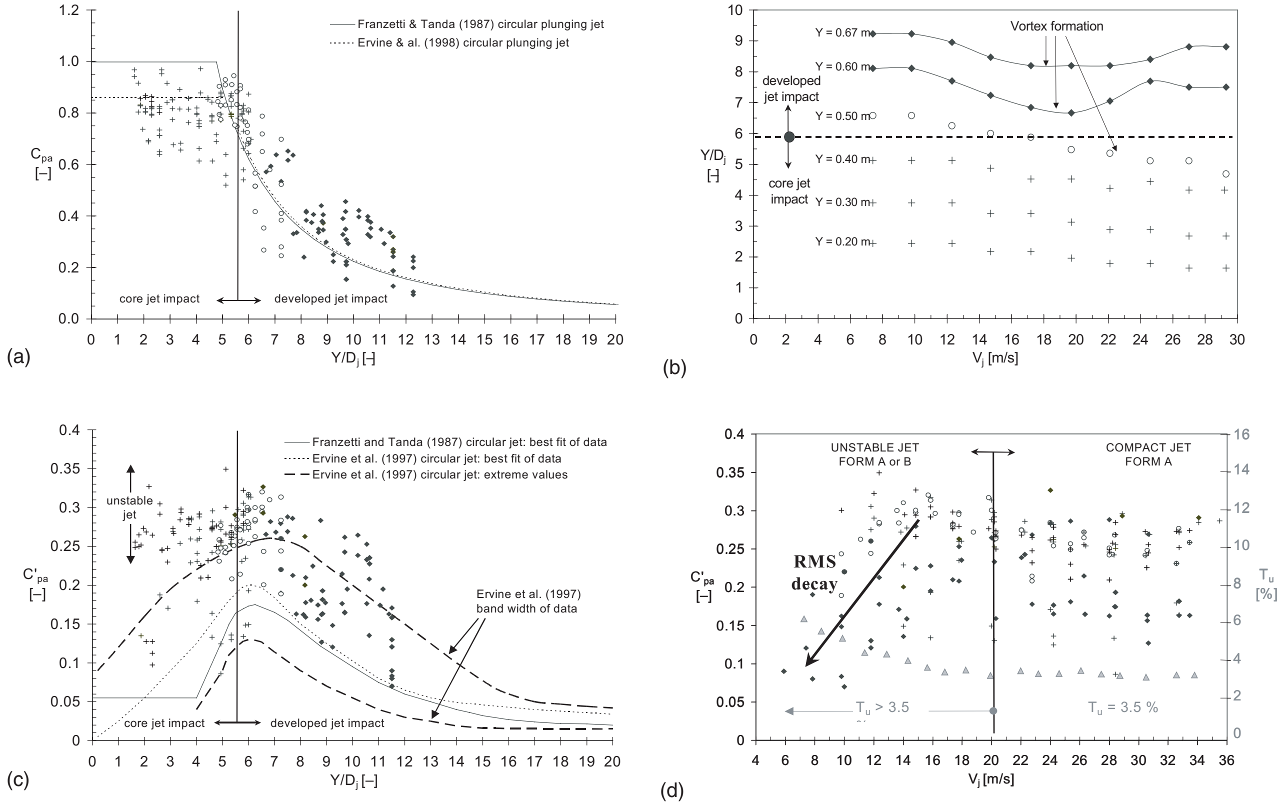

Figure 10 Non-dimensional pressure coefficients for core jet impact (pool depths of 0.20 to 0.40 m, (+)-symbol), combined core-developed jet impact (pool depth of 0.50 m, (○)-symbol) and for developed jet impact (pool depths of 0.60 to 0.67 m, (♦)-symbol): (a) C_{pa} as a function of Y/D_j ratio; (b) Y/D_j ratio as a function of mean jet velocity V_j; (c) C'_{pa} as a function of Y/D_j ratio; (d) C'_{pa} as a function of mean jet velocity V_j.

Table 2 Comparison of turbulent energy distribution with frequency for low and high-velocity jets.

Frequency range		$V_j = 7.4$ m/s	$V_j = 29.3$ m/s	Energy difference
Description	Hz	(%)	(%)	(%)
Low macro-turbulent frequencies	1–20	77	39	−38
Intermediate frequencies	21–100	18	50	+32
High frequencies	101–200	4	10	+6

where the turbulent energy distribution as a function of frequency is compared for low and high jet velocities. Low velocity jets have almost 80% of their turbulent energy at low frequencies (between 1 and 20 Hz, corresponding to the macroturbulent range). High velocity jets have less than 40% of their turbulent energy at low frequencies and more than 60% at higher frequencies. In other words, by using near-prototype jet velocities, about half of the turbulent energy that was available at low frequencies has been transferred towards higher frequencies. The intermediate frequency range of 20–100 Hz thereby receives most of this energy transfer and represents half of the total turbulent energy.

Extreme pressure values are described by the following dimensionless pressure coefficients:

$$C^{+}_{pa} = \frac{H_{max} - H_m}{\varphi \cdot V_j^2/2g} \tag{3}$$

and

$$C^{-}_{pa} = \frac{H_m - H_{min}}{\varphi \cdot V_j^2/2g} \tag{4}$$

with H_{max} and H_{min} the maximum and minimum measured dynamic pressure heads (in [m]). Extreme positive values occur at Y/D_j ratios of 10, in agreement with existing data (Ervine *et al.*, 1997) (Fig. 11a). Extreme negative values occur for a Y/D_j ratio of 4 to 6, but stay more or less constant for lower Y/D_j ratios. This is in contradiction with the data by Ervine *et al.* (1997) (Fig. 11b).

The measured extreme pressure values have been found higher than the best-fit curve defined by Ervine *et al.* (1997). This again is probably caused by the use of near-prototype jet velocities and a more correct simulation of intermediate and high frequencies on the present test facility (Bollaert *et al.*, 2002).

The measured pool bottom pressures have also been investigated by use of the probability density function (PDF). The normalization of histograms, using their mean value μ and standard deviation σ as a function of the Y/D_j ratio, allows to compare the PDF's of core and developed jets with a Gaussian distribution (Fig. 11c). Figure 11c presents a series of PDF's measured for core and developed jets and for different jet velocities. The PDF's for developed jets are positively skewed, with a low median pressure alternated by a significant amount of very high pressures. This dispersed pressure pattern favors the presence of air bubbles in rock joints.

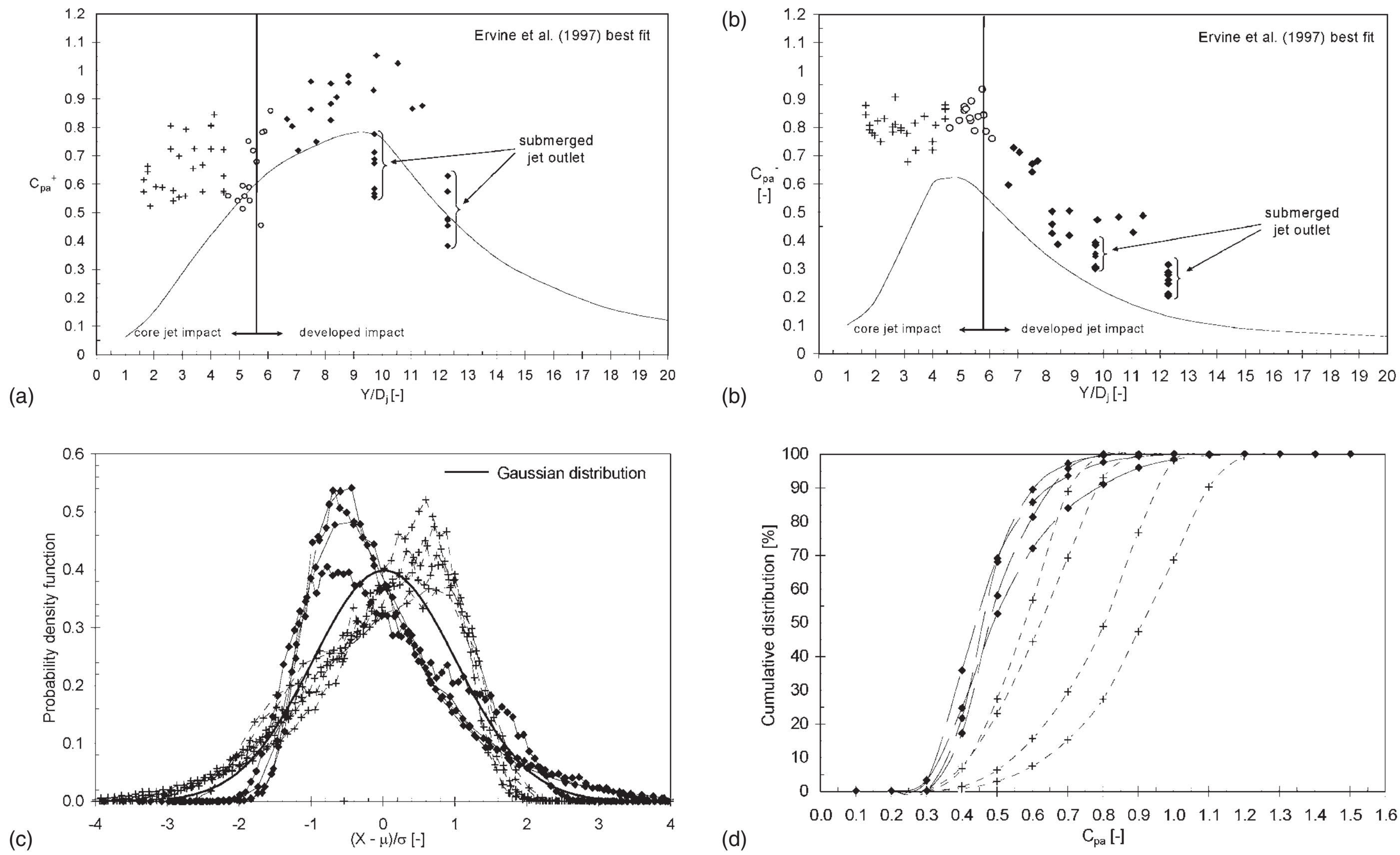

Figure 11 Maximum and minimum pressure coefficients measured at the plunge pool bottom for core jet impact (pool depths of 0.20–0.40 m, (+)-symbol), combined core-developed jet impact (pool depth of 0.50 m, (○)-symbol) and developed jet impact (pool depths of 0.60–0.67 m, (♦)-symbol): (a) C_{pa}^{+} as a function of Y/D_j; (b) C_{pa}^{-} as a function of Y/D_j; (c) probability density functions (PDF) compared to the Gaussian distribution; (d) cumulative distribution (in [%]) with respect to the C_p value of the measured pressures.

On the other hand, core jets generate a negatively skewed PDF at the pool bottom. This results in a high median value, as can be intuitively predicted. Although, occasional pressure drops are still present. The air content inside the joint corresponds to the air that is in solution in the core of the jet (∼0.5–1%), and not to the air in the highly aerated plunge pool shear layer (∼10–20%). Thus, much less air is available in underlying rock joints. This results in high pressure wave celerities and resonance frequencies of the joints. High resonance frequencies means that pressure amplification inside the joint is hardly possible. The difference in median pressure value between core and developed jets is also illustrated in Fig. 11d, which presents the cumulative distribution as a function of C_{pa}.

6.2 *Dynamic pressures in rock joints*

The mean (C_{pd}), RMS (C'_{pd}) and extreme positive (C_{pd}^{+}) dynamic pressure coefficients have been determined at the end (sensor (d)) of the 1D joint (Figs. 12a, c and e, left-hand side of figure) and the 2D joint (Figs. 12b, d and f, right-hand side of figure).

The 1D joint produces C_{pd} values that are similar to the C_{pa} values at the pool bottom as presented in Fig. 10a. On the other hand, the C'_{pd} values are substantially higher than the C'_{pa} values, as a result of the modulation of the pool bottom pressures into oscillatory and resonance pressure waves inside the joint (Fig. 12c). The dependence of C'_{pd} on the Y/D_j ratio follows the same trend as was observed for pool bottom fluctuations, i.e. a rapid increase up to Y/D_j ratios of 6 to 8, followed by a continuous decrease for higher ratios (Fig. 12c).

In the 2D joint, for core jet impact, the C_{pd} values are much lower than the C_{pa} values. For developed jet impact, both C_p values are similar (Fig. 12b). This is due to the fact that core jet impact has a locally high centerline mean pressure, combined with a strong radial decrease of this mean pressure.

The jet's centerline C_{pa} value doesn't cover the whole width of the rock joint entrance. Therefore, important diffusive effects occur inside the joint. For developed jet impact, however, the shear layer covers almost the whole joint entrance, and the radial decrease of the mean dynamic pressure is much less pronounced. Thus, a homogenously distributed mean pressure acts all over the pool bottom and inside the rock joint (Fig. 12b). The RMS values for the 2D joint are lower than the ones for the 1D joint, for both core and developed jets (Fig. 12d). In the core impact region, C'_{pd} is nearly constant (=0.10). In the developed jet impact region, a decrease with Y/D_j can be observed, tendency that is similar to the mean dynamic pressure evolution (Fig. 12b).

Peak pressures are of interest when applying a rock mass failure criterion, such as tensile failure or fracture mechanics, in order to assess scour formation. In the following, only positive extreme values (C_{pd}^{+}) are discussed because they are relevant to such failure criteria. At the end position inside the 1D joint, dynamic pressure amplifications of up to 4–5 times

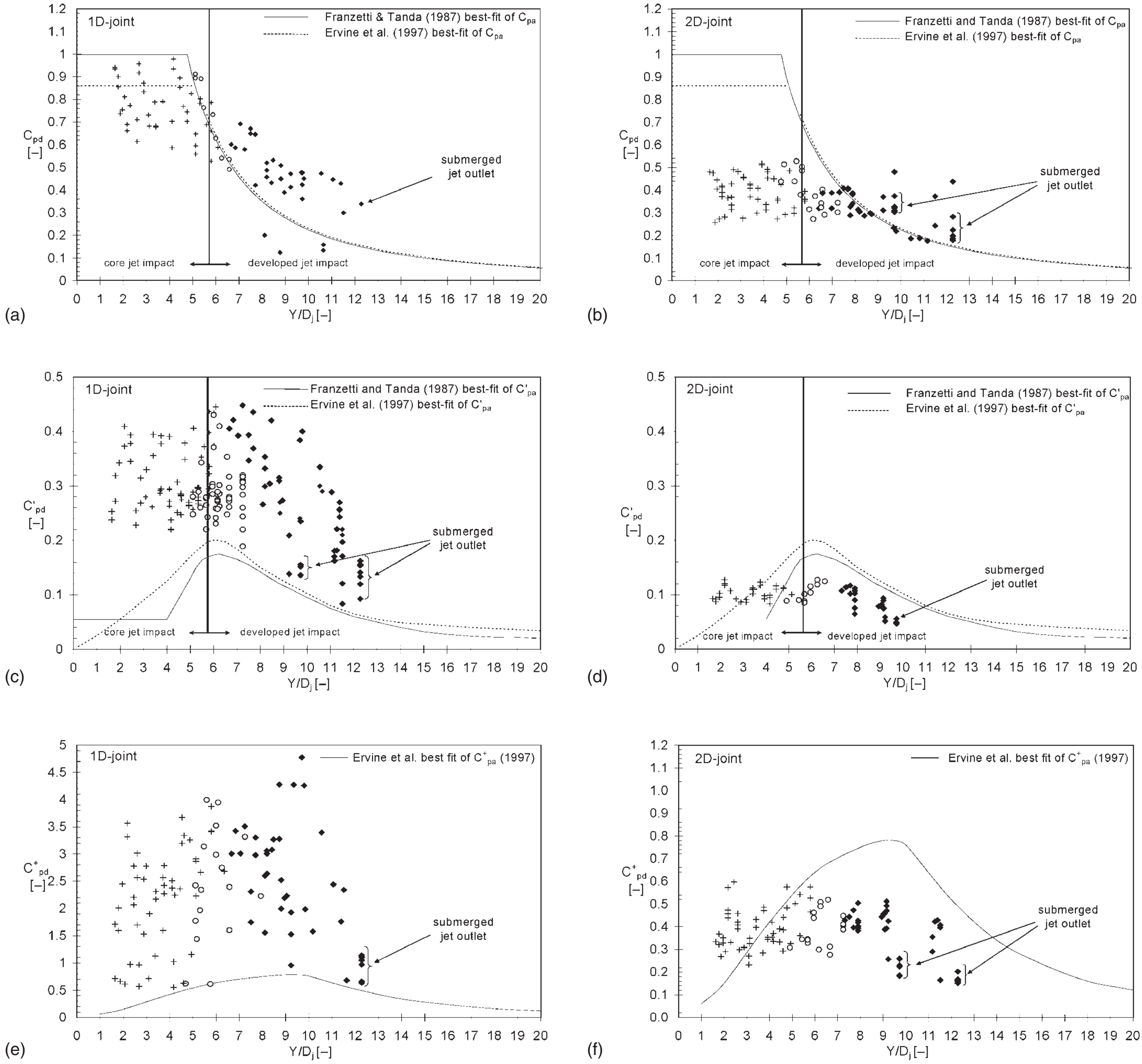

Figure 12 Non-dimensional mean, RMS and extreme pressure coefficients at the end of a rock joint (sensor (d)) as a function of the Y/D_j ratio, for core jet impact (pool depths of 0.20–0.40 m, (+)-symbol), combined core-developed jet impact (pool depth of 0.50 m, (○)-symbol) and developed jet impact (pool depths of 0.60–0.67 m, (♦)-symbol): (a) 1D joint: C_{pd}-coefficient; (b) 2D joint: C_{pd}-coefficient; (c) 1D joint: C'_{pd}-coefficient; (d) 2D joint: C'_{pd}-coefficient; (e) 1D joint: C^+_{pd}-coefficient; (f) 2D joint: C^+_{pd}-coefficient. Comparison with available literature data of pool bottom pressures (Franzetti and Tanda, 1987; Ervine *et al.*, 1997).

the incoming kinetic energy ($\varphi \cdot V_j^2/2g$) have been observed (Fig. 12e).

At the end position inside the 2D joint, measured extremes have been found up to only 0.6 times the incoming kinetic energy. The highest extremes were thereby obtained for core jet impact. It is particularly interesting to notice the agreement between RMS values and extreme values, for both core and developed jet impact.

The PDF's inside the 1D joint have been studied by distinguishing high (>15–20 m/s, Fig. 13a) and low (up to 15 m/s, Fig. 13b) velocities of the jet at impact. For high jet velocities, two completely different PDF's are observed. Developed jet impact is positively skewed, indicating a low median pressure and a lot of peak values due to resonance phenomena. Core jet impact is characterized by a negatively skewed PDF, with a high median pressure and almost no high values or resonance effects. For low jet velocities, only positively skewed PDF's are observed inside the 1D joint. Therefore, resonance is present for both jet impact cases (Fig. 13b).

An attempt has been made to relate the peak pressures inside the joints (C^+_{pd}) to the corresponding RMS values (C'_{pa}) at the plunge pool bottom. This reflects the degree of pressure amplification inside the joint and has been done for the 1D joint by means

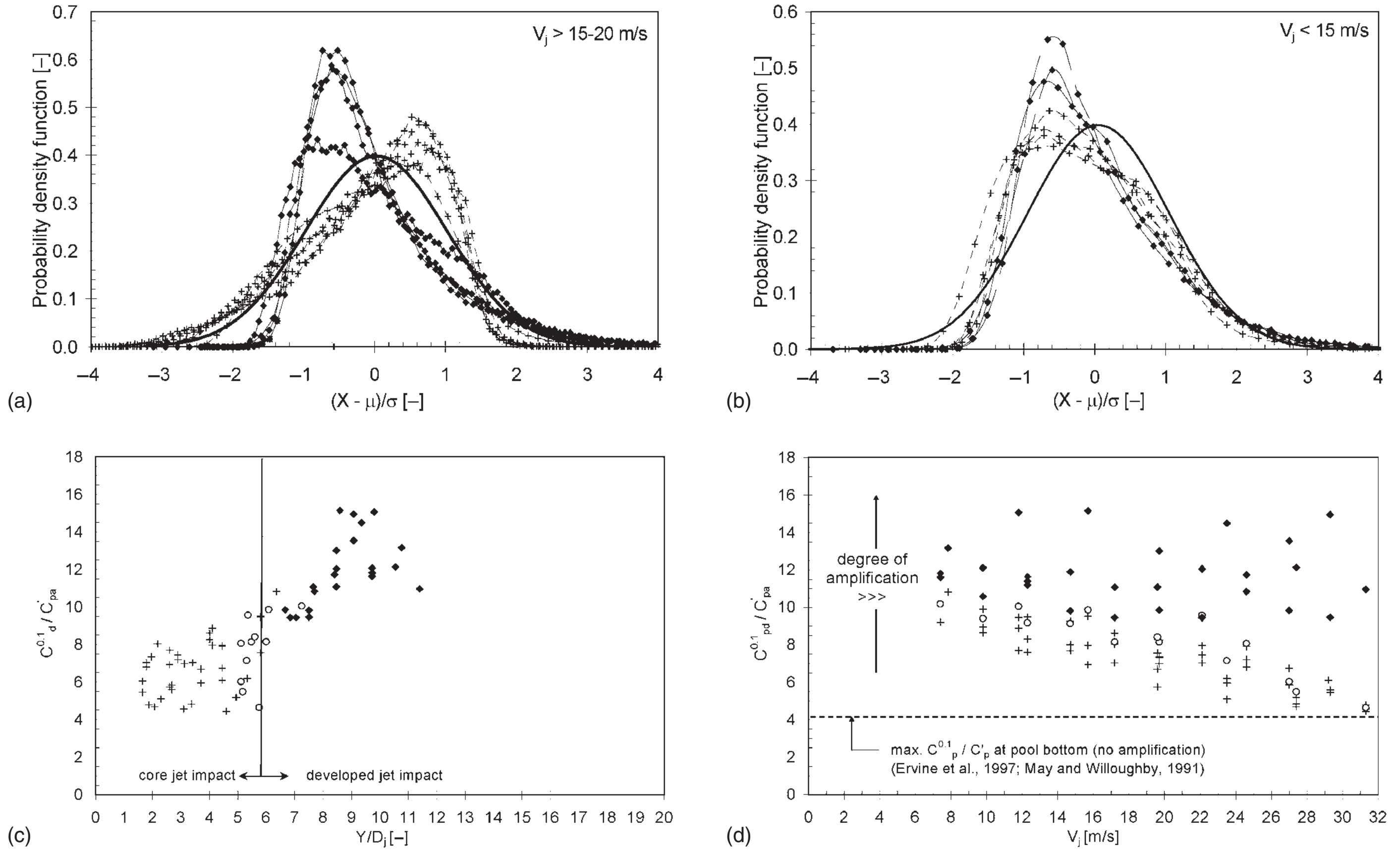

Figure 13 Time domain pressure analysis in a 1D joint, for core jet impact ((+)-symbol), combined core-developed jet impact ((○)-symbol) and developed jet impact ((♦)-symbol): (a) Probability density function (PDF) at jet velocities > 15–20 m/s; (b) Probability density function (PDF) at jet velocities up to 15 m/s; (c) Amplification coefficient $C_d^{0.1}/C'_{pa}$ as a function of Y/D_j; (d) Amplification coefficient $C_d^{0.1}/C'_{pa}$ as a function of jet velocity V_j.

of the amplification ratio $C_{pd}^{0.1}/C'_{pa}$. This ratio expresses the pressure with a 0.1% probability of occurrence at the joint-end divided by the RMS value of the pressure fluctuations at the plunge pool bottom (Figs. 13c and d). The ratio has values between 4 and 10 for core jet impact and between 8 and 16 for developed jet impact. A typical ratio of extreme values to RMS values at a plunge pool bottom is only 3 to 4 (May and Willoughby, 1991; Ervine *et al.*, 1997). It may be concluded that core jet impact exhibits significant amplification for low jet velocities, as shown by the transfer function in Fig. 7e. At high jet velocities, the amplification tends towards a value of 4, characteristic for pool bottom pressures. Developed jet impact presents amplification independent of the jet velocity at impact (Fig. 13d).

7 Conclusions

Fluctuating pressures generated by high velocity jet impact have been simultaneously measured at a modeled plunge pool bottom and inside artificially created 1D and 2D closed end rock joints. The pressures have been analyzed in the frequency domain, based on the spectral density and the transfer function, and in the time domain, by the mean, RMS and extreme pressures, as well as by probability density distributions.

For 1D rock joints, it has been found that high velocity plunging jets have the potential to generate significant oscillatory and resonance pressures inside underlying joints. These highly non-linear phenomena travel at wave celerities that are strongly influenced by the air concentration of the joints. This content depends on the air concentration of the plunge pool and on pressure fluctuations inside the joint. It continuously changes as a function of time and space, according to basic physical laws.

A different behavior between core jets and developed jets has been identified. Core jets generate high pressures with low fluctuations. Therefore, low air concentrations are typical (<1%). At high jet velocities, core jet impact transfers high pressures inside the joint, which results in high wave celerities and high resonance frequencies. Consequently, the jet cannot create sufficient spectral energy at these frequencies to stimulate the joint to resonance pressures. On the other hand, developed jet impact generates a pressure pattern with frequent pressure fluctuations and is influenced by the high air content present in the plunge pool shear layer. Therefore, high air concentrations can be observed (up to 10–20%), resulting in very low wave celerities (even at high jet velocities). For such conditions, the resonance frequencies of the joint are low and correspond to frequencies that are easily generated by the jet. The pool bottom pressure fluctuations are transformed inside the joint into an alternation of peak pressures and periods of very low pressures. Measured pressure peaks (for a 0.1% probability of occurrence) were up to 16 times the RMS value at the pool bottom, or up to 4–5 times the incoming kinetic energy of the jet.

For 2D rock joints, the jet at impact doesn't cover the whole width of the joint and is not able to generate such extremely high pressures inside the joint (2D diffusive effects). However, high air contents of up to 10–20% have been observed, as well as clearly distinguishable resonance frequencies. This is valid for both core and developed jets.

It is believed that the jets generated by the test facility are representative for prototype jets issuing from any type of outlet structure (overflow weir, pressurized outlet, ski-jump, …). The type of outlet structure can be accounted for by adapting the initial turbulence intensity Tu of the jet. For practice, the dynamic pressures measured on the test facility for the highest jet velocities and for developed jets are considered most appropriate. The use of near-prototype jet velocities guarantees a minimization of eventual turbulence and aeration scaling effects. For core jet impact, it is recommended to use the results obtained for developed jet impact. This is because it is believed that real-life core jet impact is characterized by both high jet velocities and low-frequency instabilities of the core of the jet. Core instabilities are an artifact of the present test facility but can nevertheless also be observed on prototype jets. Based on the present test results, these instabilities generate pressure fluctuations at the pool bottom that are typical for developed jet impact. Their significance for prototype core jets is not clear yet and merits to be investigated. In the mean time, it is proposed to apply the pressure fluctuations that are representative for developed jets, because these are much more dangerous to the underlying rock mass.

In conclusion, dynamic pressures acting at a plunge pool bottom, due to high velocity jet impact, exhibit significant transient amplification when transferred into underlying 1D closed end rock joints. This is a key element for a physically better understanding of rock mass destruction. Applying transient pressures in 1D joints to a rock mass failure criterion, such as tensile break-up or fracture mechanics, may form the basis for a more appropriate and physically-based estimation of the ultimate scour depth in fractured media.

Acknowledgments

The authors gratefully thank the anonymous reviewers for their suggestions and recommendations that have strengthened the paper. This research project has been partially funded by the Swiss Commission on Technology and Innovation (CTI), involving the Swiss Committee on Dams (CSB) and Stucky Consulting Engineers. Special thanks go to Dr. H. T. Falvey for his valuable suggestions and insight in this field.

Notations

c = pressure wave celerity [m/s]
c_{mean} = mean pressure wave celerity in rock joint [m/s]
f = frequency of pressure fluctuations [Hz]
f_{res} = fundamental resonance frequency of joint [Hz]
g = gravitational acceleration [m/s^2]
p = pressure value [Pa] or [m]
p_m = mean pressure value [Pa] or [m]
p_{abs} = absolute pressure value [Pa] or [m]
C_{px} = mean dynamic pressure coefficient (x = sensor position) [-]
C'_{px} = root-mean-square dynamic pressure coefficient (x = sensor position) [-]
C^+_{px} = positive dynamic pressure coefficient (x = sensor position) [-]
C^-_{px} = negative dynamic pressure coefficient (x = sensor position) [-]
$C^{0.1}_{px}$ = 0.1% probability dynamic pressure coefficient (x = sensor position) [-]
D_j = mean jet diameter at impact [m]
E_{st} = modulus of elasticity of steel bars [GPa]
H = incoming total pressure head or kinetic energy of jet ($=V_j^2/2g$) [m]
H_m = mean dynamic pressure head [m]
H' = RMS value of dynamic pressure fluctuations [m]
H_{max} = maximum dynamic pressure head [m]
H_{min} = minimum dynamic pressure head [m]
L_b = jet break-up length [m]
L_f = length of rock joint [m]
L = jet fall height [m]
Q_a = air discharge [m^3/s]
Q_w = water discharge [m^3/s]
RMS = root-mean-square values of pressure fluctuations [m]
$S_{h,p}$ = $f \cdot Y/V_j$, Strouhal number of plunge pool [-]
$S_{xx}(f)$ = power spectral density of pressure fluctuations [m^2/Hz]
Tu = initial jet turbulence intensity [%]
V_j = mean jet outlet velocity [m/s]
Y = plunge pool water depth [m]
α = air concentration [%]
α_j = air concentration at jet impact in plunge pool [%]
α_f = air concentration in rock joint [%]
β = volumetric air-to-water ratio ($= Q_a/Q_w$) [-]
δ_{out} = outer spread angle of plunging jet [°]
φ = parameter for non-uniform velocity distribution [-]
σ = standard deviation of pressure fluctuations [m]
σ^2 = variance of pressure fluctuations [m^2]

References

1. BALLIO, F., FRANZETTI, S. and TANDA, M.G. (1994). "Pressure Fluctuations Induced by Turbulent Circular Jets Impinging on a Flat Plate," *Excerpta*, 7, 41–59.
2. BEARMAN, P.W. (1972). "An Investigation of the Forces on Flat Plates Normal to a Turbulent Flow," *J. Fluid Mech.*, 46, 177–198.
3. BIN, A.K. (1984). Air entrainment by plunging liquid jets, *Proceedings of the IAHR Symposium on scale effects in modeling hydraulic structures*, Esslingen.
4. BOLLAERT, E. (2001). Spectral density modulation of plunge pool bottom pressures inside rock fissures, *Proceedings of the XXIXth IAHR Congress*, Student Paper Competition, Beijing, China.

5. Bollaert, E. and Schleiss, A. (2001a). Air bubble effects on transient water pressures in rock fissures due to high velocity jet impact, *Proceedings of the XXIXth IAHR Congress*, Beijing, China.
6. Bollaert, E. and Schleiss, A. (2001b). A new approach for better assessment of rock scouring due to high velocity jets at dam spillways, *Proceedings of the ICOLD European Symposium*, Geiranger, Norway.
7. Bollaert, E., Falvey, H.T. and Schleiss, A. (2002). Assessment of turbulent jet impingement in plunge pools: the particular characteristics of a near-prototype physical model study, *Proceedings of Riverflow 2002*, Louvain-la-Neuve, Belgique.
8. Bollaert, E. (2002). Transient water pressures in joints and formation of rock scour due to high-velocity jet impact, *Communication No. 13*, Laboratory of Hydraulic Constructions, EPFL, Switzerland.
9. Ervine, A. (1998). "Air Entrainment in Hydraulic Structures: A Review," *Proceedings Institution of Civil Engineers. Wat., Marit. & Energy*, 130, 142–153.
10. Ervine, D.A. and Falvey, H.T. (1987). Behavior of turbulent water jets in the atmosphere and in plunge pools, *Proceedings Institution of Civil Engineers*, Part 2, Vol. 83, pp. 295–314.
11. Ervine, D.A., Falvey, H.R. and Withers, W. (1997). "Pressure Fluctuations on Plunge Pool Floors," *J. Hydr. Res.*, IAHR, 35(2), 257–279.
12. Franzetti, S. and Tanda, M.G. (1987). Analysis of turbulent pressure fluctuation caused by a circular impinging jet, *International Symposium on New Technology in Model Testing in Hydraulic Research*, India, pp. 85–91.
13. Hinze, J.O. (1959). Turbulence. McGraw-Hill.
14. Huot, J.P., Rey, C. and Arbey, H. (1986). "Experimental Analysis of the Pressure Field Induced on a Square Cylinder by a Turbulent Flow," *J. Fluid Mech.*, 162, 283–298.
15. Mason, P.J. (1989). "Effects of Air Entrainment on Plunge Pool Scour," *J. Hydr. Engrg.*, ASCE, 115(3), 385–399.
16. Toso, J.W. and Bowers, C.E. (1988). "Extreme Pressures in Hydraulic Jump Stilling Basins," *J. Hydr. Engrg.*, ASCE, 114(8), 829–843.
17. Van De Sande, E. and Smith, J.M. (1973). "Surface Entrainment of Air by High Velocity Water Jets, *Chemical Engineering Science*, 28, 1161–1168.
18. Wylie, E.B. and Streeter, V.L. (1978). Fluid transients, McGraw-Hill, United States.